Spatially complex localization in twisted elastic rods constrained to an elliptic cylinder

Jingjing Feng[1,2], Qichang Zhang[1,2] and Wei Wang[1,2]

[1] Department of Mechanics, School of Mechanical Engineering, Tianjin University, Tianjin, China

[2] Tianjin Key Labortory of Nonlinear Dynamics and Chaos Control, Tianjin University, Tianjin, China

E-mail: jjfeng@tju.edu.cn

Abstract. In molecular biology, the elastic rod is wound on the elliptic cylinder can be used as a simplified model of the DNA and protein molecules, in which the elliptic cylinder is used to simulate the heterogeneity of the protein molecules. The problem can be described as a long thin weightless rod constrained, by suitable distributed forces, to lie on an elliptic cylinder while being held by end tension and twisting moment. The Cosserat director theory is used to formulate this problem. More complicated shaped are possible and special attention is given to localized configurations described by homoclinic and heteroclinic orbits of the oscillator. The analytical results of homoclinic and heteroclinic boundary conditions are obtained from Padé approximation. By using the analytical results of homoclinic and heteroclinic solution, both internal force and 3D configuration are discussed in detail. The results of analytical and numerical integration are compared to verify the effectiveness and feasibility of the analytical method.

1. Introduction

In molecular biology, wounded elastic rod in a cylinder can be used as a simplified model of the combination of DNA and protein molecules. This model also has a wide range of applications in other areas, for example, considering drill strings constrained to lies within a cylindrical bore hole [1, 2] in the oil drilling industry. Taking the heterogeneity of the protein molecules into account, we can simplify the model into elastic rod constrained to lie on an elliptic cylinder, where non-circular cross-section of elliptic cylinder is used to simulate protein molecules

The localized buckling of long, thin, initially straight, elastic rods subject to end forces and moments for the case of rods with non-symmetric cross section was studied numerically [3]. The circle of homoclinic orbits present in the symmetric case breaks up and four isolated primary homoclinic orbits were left in breaking the rotational symmetry by considering rods with different bending stiffnesses in two orthogonal directions [4]. The heteroclinic saddle connections are found to play an important role in the post-buckling behavior by defining critical loads at which a straight isotropic rod may coil up into a helix [5]. The anisotropic rod constrained to a cylinder was analyzed by numerical methods [6]. And same results are similar with the isotropic rod constrained to the plane[7].

In the construction of the homoclinic and heteroclinic orbits in nonlinear dynamical systems, numerical simulations are used in most cases. While on contrast the analytical approach. The

analytical approaches are rare for constructing the homoclinic and heteroclinic orbits in nonlinear dynamical systems, and numerical simulations are frequently used. The Padé approximants were successfully used for the homoclinic orbits of two-dimensional axisymmetric breathers by Vakakis [8]. The quasi-Padé approximants were used to construct the homoclinic orbits in nonlinear Schrodinger equation system by Mikhlin [9]. The analytic homoclinic orbits, in the non-autonomous Duffing equation and the Van Der Pol-Duffing equation with weakly coupled nonlinear oscillators, were computed in Ref. [10]. The Padé approximation is extended to be used to construct the homoclinic and heteroclinic orbits in the asymmetric systems, which to improve the accuracy of the threshold for the onset of chaos [11-13]. However, the problem of effective analytic approximate of the heteroclinic orbits is difficult and it is not solved up to now.

Attention is also given to localized rod solutions corresponding to homoclinic orbits of the oscillator. But the heteroclinic orbits are special phenomenon which is not presented in the free rod case. They play an important role in the behavior of solutions by defining critical loads at which a straight rod may coil up into a helix. According to the radius of the elliptic cylinder, the heteroclinic orbits occur.

2. Model

The equilibrium equations of the constrained rod are given by[14]

$$\begin{cases} \dot{\vec{n}} = \vec{f}, \\ \dot{\vec{m}} + \dot{\vec{r}} \times \vec{n} = 0, \\ \dot{\vec{r}} = \vec{d}_3, \\ \dot{\vec{d}}_i = \vec{u} \times \vec{d}_i, \end{cases} \tag{1}$$

where $\vec{n}$ and $\vec{f}$ are internal forces and moments along the rod respectively, and $\{\vec{d_1}, \vec{d_2}, \vec{d_3}\}$ is the director frame. The vector $\vec{d_3}$ is taken to be tangent to the rod, where the vector function $\vec{r}$ describes the centerline of the rod relative to some fixed co-ordinate system to be specified later. And the directors $\vec{d_1}$ and $\vec{d_2}$ are chosen along the principal axes of the second moment of area in the normal cross-section of the rod.

The generalized strain vector

$$\vec{u} = u_1\vec{d}_1 + u_2\vec{d}_2 + u_3\vec{d}_3, \tag{2}$$

satisfies the generalized stresses and strains

$$u_1 = \frac{1}{B_1}\vec{m}\cdot\vec{d}_1, \qquad u_2 = \frac{1}{B_2}\vec{m}\cdot\vec{d}_2, \qquad u_3 = \frac{1}{C}\vec{m}\cdot\vec{d}_3, \tag{3}$$

where B_1 and B_2 are the bending stiffnesses about $\vec{d}_1$ and $\vec{d}_2$, respectively, and C is the torsional stiffness.

Considering $\{\vec{e_1}, \vec{e_2}, \vec{e_3}\}$ is a fixed right-handed orthonormal co-ordinate system, we introduce the position vector of the elliptic cylindrical coordinates (R, ψ, z) based on the cylindrical coordinate

$$\vec{r} = R\cos\psi\vec{e}_1 + R\sin\psi\vec{e}_2 + z\vec{e}_3, \tag{4}$$

which meet

$$\begin{cases} R = r\sqrt{\cos^2\psi_0 + \dfrac{b^2}{a^2}\sin^2\psi_0}, \\ \tan\psi = \dfrac{b}{a}\tan\psi_0, \end{cases} \tag{5}$$

where a is the semi-mahor axis of unit elliptical column in $\vec{e}_1$ direction and b is the semi-minor axis in $\vec{e}_2$ direction. And circumferential angle of unit cylinder ψ_0 is introduced. After that, elliptical coordinate system $\{\vec{e_r},\vec{e_\psi},\vec{e_z}\}$ can be written in the following form,

$$\begin{cases}\vec{e_r} = a\cos\psi_0\vec{e_1} + b\sin\psi_0\vec{e_2},\\ \vec{e_\psi} = -a\sin\psi_0\vec{e_1} + b\cos\psi_0\vec{e_2},\\ \vec{e_z} = \vec{e_3},\end{cases} \tag{6}$$

where $\vec{e_r}$ is normal to the cylinder, $\vec{e_\psi}$ is the circumferential direction, and $\vec{e_z}$ is the direction of the axis of the elliptical column. And there are

$$\begin{aligned}\vec{r} &= ra\cos\psi_0\vec{e}_1 + rb\sin\psi_0\vec{e}_2 + z\vec{e}_3\\ &= r\vec{e}_r + z\vec{e}_z,\end{aligned} \tag{7}$$

which also meets the following changes

$$\begin{cases}\dot{\vec{e}}_r = -\dot{\psi}_0 a\sin\psi_0\vec{e}_1 + \dot{\psi}_0 b\cos\psi_0\vec{e}_2 = \dot{\psi}_0\vec{e}_\psi,\\ \dot{\vec{e}}_\psi = -\dot{\psi}_0 a\cos\psi_0\vec{e}_1 - \dot{\psi}_0 b\sin\psi_0\vec{e}_2 = -\dot{\psi}_0\vec{e}_\psi.\end{cases} \tag{8}$$

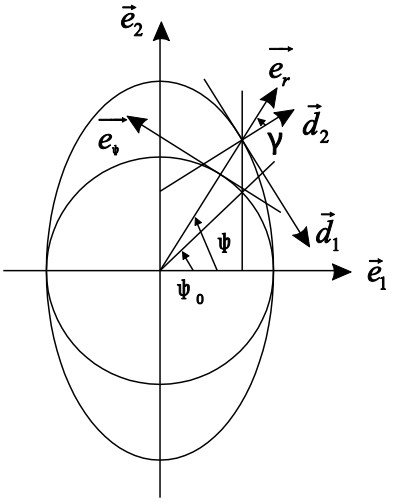

Figure 1 elliptic cylindrical coordinate

Define $\vec{n} = n_r\vec{e}_r + n_\psi\vec{e}_\psi + n_z\vec{e}_z$, $\vec{m} = m_r\vec{e}_r + m_\psi\vec{e}_\psi + m_z\vec{e}_z$, $\vec{d}_i = d_{ir}\vec{e}_r + d_{i\psi}\vec{e}_\psi + d_{iz}\vec{e}_z$ $(i=1,2,3)$. From $\dot{\vec{r}} = \vec{d}_3$ we have

$$\begin{cases}\dot{\psi}_0 = \dfrac{d_{3\psi}}{r},\\ \dot{r} = d_{3r},\end{cases} \tag{9}$$

from the components of $\vec{d}_3$, the following equations (10) can be obtained. The external normal reaction force can be written as $\vec{f} = f\vec{e}_r$.

$$\begin{cases} \dot{d}_{3r} = \dfrac{d_{3\psi}^2}{r} + u_2 d_{1r} - u_1 d_{2r}, \\ \dot{d}_{3\psi} = -\dfrac{d_{3r} d_{3\psi}}{r} + u_2 d_{1\psi} - u_1 d_{2\psi}, \\ \dot{d}_{3z} = u_2 d_{1z} - u_1 d_{2z}. \end{cases} \tag{10}$$

Constraint condition is that along the centerline of the elliptical column conserved $\dot{r} = d_{3r} \equiv 0$, namely

$$\frac{d_{3\psi}^2}{r} + u_2 d_{1r} - u_1 d_{2r} \equiv 0. \tag{11}$$

Considering $\dot{\vec{n}} = \vec{f}$, equation is obtained,

$$\begin{cases} \dot{n}_r = f + \dfrac{d_{3\psi} n_\psi}{r}, \\ \dot{n}_\psi = -\dot{\psi}_0 n_r, \\ \dot{n}_z = 0. \end{cases} \tag{12}$$

Introduce a new function h which is defined by

$$\dot{h} = f + \frac{d_{3\psi} n_\psi}{r}, \tag{13}$$

and the transformation is,

$$\begin{cases} \bar{n}_r = n_r - h, \\ \bar{n}_\psi = n_\psi, \\ \bar{n}_z = n_z. \end{cases} \tag{14}$$

That is $\dot{\bar{n}}_r = 0$ and $\dot{\bar{n}}_z = 0$. Considering the side force, $\bar{n}_z = T$ is obtained. And let $\bar{n}_r = 0$, h can be determined in the equation(13). Then moment equation is

$$\dot{\vec{m}} = -\vec{d}_3 \times \bar{n} - h\vec{d}_3 \times \vec{e}_r. \tag{15}$$

The director frame $\{\vec{d_1}, \vec{d_2}, \vec{d_3}\}$ can be expressed in the following form with Euler angle θ, ϕ,

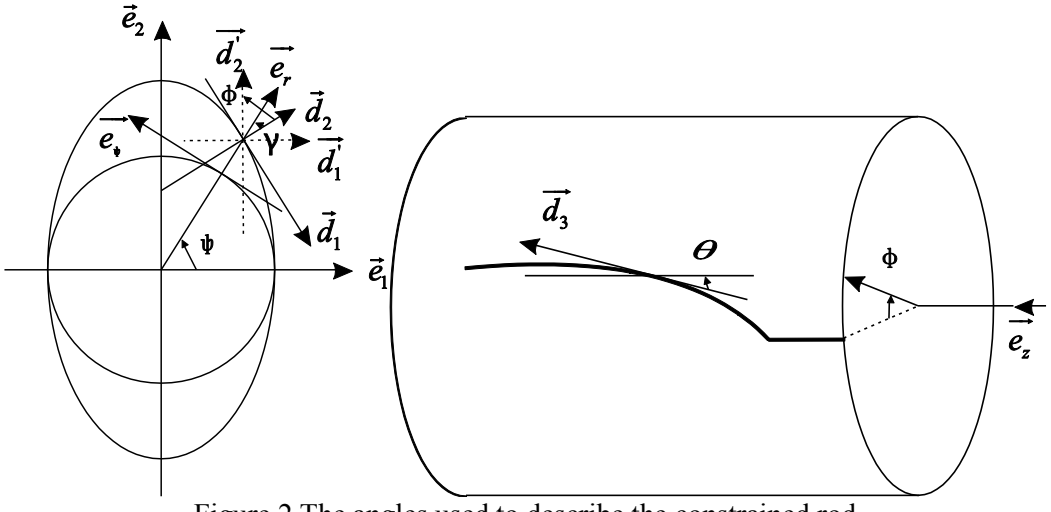

Figure 2 The angles used to describe the constrained rod

$$\begin{cases} \vec{d}_1 = -\sin(\gamma-\phi)\vec{e}_r - \cos(\gamma-\phi)\cos\theta\vec{e}_\psi + \cos(\gamma-\phi)\sin\theta\vec{e}_z, \\ \vec{d}_2 = \cos(\gamma-\phi)\vec{e}_r - \sin(\gamma-\phi)\cos\theta\vec{e}_\psi + \sin(\gamma-\phi)\sin\theta\vec{e}_z, \\ \vec{d}_3 = \sin\theta\vec{e}_\psi + \cos\theta\vec{e}_z, \end{cases} \tag{16}$$

where θ measures deflection angle from centerline of the rod to centerline of elliptic cylinder, and ϕ is internal twist angle of $\vec{d_1}$ turns around $\vec{d_3}$. If rod is not internal twist, then $\phi = 0$. $\vec{d_1}$ is in tangent plane of elliptic cylinder and $\vec{d_2}$ is the corresponding normal line.

The following Eular angle expressions can be had by taking equation (16) into original equation (1),

$$\begin{cases} \dot{\theta} = u_1\sin(\gamma-\phi) - u_2\cos(\gamma-\phi), \\ \dot{\phi} - \dot{\gamma} = u_3 - \dfrac{1}{r}\sin\theta\cos\theta. \end{cases} \tag{17}$$

Introducing the dimensionless variable,

$$\begin{aligned} &x_1 = \frac{n_r}{T}, x_2 = \frac{n_\psi}{T}, x_3 = \frac{n_z}{T}, x_4 = \frac{m_r}{M}, x_5 = \frac{m_\psi}{M}, x_6 = \frac{m_z}{M}, \\ &t = \frac{M}{B_2}s, \tilde{h} = \frac{h}{T}, \tilde{f} = \frac{B_2 f}{MT} \end{aligned} \tag{18}$$

where T and M are the applied loads. According to the derivation process in front, $x_1 = \tilde{h}, x_3 = 1$ can be gained. Finally, the system (1) can be rewritten as the following dimensionless equation

$$\begin{cases} \dot{x}_2 = -\dfrac{1}{\tilde{r}}\tilde{h}\sin\theta, \\ \dot{x}_4 = -\dfrac{1}{m^2}\sin\theta + \dfrac{1}{m^2}x_2\cos\theta + \dfrac{1}{\tilde{r}}x_5\sin\theta, \\ \dot{x}_5 = -\dfrac{\tilde{h}}{m^2}\cos\theta - \dfrac{1}{\tilde{r}}x_4\sin\theta, \\ x_6 = \dfrac{\tilde{h}}{m^2}\sin\theta, \\ \dot{\theta} = -x_4 - \rho(x_4\sin^2(\gamma-\phi) + x_5\sin(\gamma-\phi)\cos(\gamma-\phi)\cos\theta - \\ \qquad x_6\sin(\gamma-\phi)\cos(\gamma-\phi)\sin\theta), \\ \dot{\phi} - \dot{\gamma} = (1+\nu)(x_5\sin\theta + x_6\cos\theta) - \dfrac{1}{\tilde{r}}\sin\theta\cos\theta, \end{cases} \tag{19}$$

where

$$m = \frac{M}{\sqrt{B_2 T}}, \rho = \frac{B_2}{B_1} - 1, \nu = \frac{B_2}{C} - 1, \tilde{r} = \frac{M}{B_2}r \tag{20}$$

are all dimensionless parameters.

Boundary constraint equation (11) may also be written as

$$\begin{aligned} &x_5\cos\theta - x_6\sin\theta + \rho(x_4\sin(\gamma-\phi)\cos(\gamma-\phi) + \\ &\quad x_5\cos^2(\gamma-\phi)\cos\theta - x_6\cos^2(\gamma-\phi)\sin\theta) + \frac{1}{\tilde{r}}\sin^2\theta = 0. \end{aligned} \tag{21}$$

Here, the solutions of equation (19) can be traced, which satisfies the condition (21). And from the third equation of (1) we can obtain,

$$\begin{cases} \dot{\psi}_0 = \dfrac{1}{\tilde{r}}\sin\theta, \\ \dot{z} = \cos\theta. \end{cases} \tag{22}$$

In the coordinate system $\{\vec{e_1}, \vec{e_2}, \vec{e_3}\}$ there are

$$\begin{cases} x = R\cos\psi = \tilde{r}a\cos\psi_0, \\ y = R\sin\psi = \tilde{r}b\sin\psi_0. \end{cases} \tag{23}$$

Two integral can be obtained from system (19).

$$\mathrm{I}_1 = \tilde{r}x_2 + m^2 x_6 = \text{constant}. \tag{24}$$

This integral equation represents the axial moment equilibrium. The second integral derivated from the "Hamiltonian"

$$\begin{aligned} \mathrm{I}_2 = {} & \frac{1}{2}(1+\rho)[-x_4\sin(\gamma-\phi) - x_5\cos(\gamma-\phi)\cos\theta + x_6\cos(\gamma-\phi)\sin\theta]^2 \\ & + \frac{1}{2}[x_4\cos(\gamma-\phi) - x_5\sin(\gamma-\phi)\cos\theta + x_6\sin(\gamma-\phi)\sin\theta]^2 \\ & + \frac{1}{2}(1+\nu)(x_5\sin\theta + x_6\cos\theta)^2 + \frac{\cos\theta}{m^2} + \frac{x_2\sin\theta}{m^2} = \text{constant}. \end{aligned} \tag{25}$$

In circular cross section, the third integral is provided by conservative torque u_3,

$$\mathrm{I}_3 = x_5\sin\theta + x_6\cos\theta = \text{constant}. \tag{26}$$

3. Analysis on the circular cross section of rod

System (19) is integrable which is made from the three integral in circular cross section mentioned above, and after simplification the following differential equations can be obtained,

$$\frac{1}{2}\dot{\theta}^2 + V(\theta) = H, \tag{27}$$

where

$$V(\theta) = \frac{\cos\theta}{m^2} + \frac{K_1\sin\theta}{\tilde{r}m^2} - \frac{K_3\sin\theta\cos\theta}{\tilde{r}} + \frac{\cos^2\theta}{\tilde{r}^2} - \frac{\cos^4\theta}{2\tilde{r}^2}, \tag{28}$$

$$H = K_2 - \frac{1}{2}K_3^2(1+\nu) + \frac{1}{2\tilde{r}^2}. \tag{29}$$

Boundary conditions are K_1, K_2 and K_3, which is the value of first integral I_1, I_2 and I_3 respectively. In arbitrary parameter values condition, the system (19) has trivial solution,

$$x_2 = 0, x_4 = 0, x_5 = 0, x_6 = 1, \theta = 0, \dot{\phi} = 1+\nu, \tag{30}$$

meanwhile $\tilde{h} = 0$. At the same time, according to the boundary conditions, system (19) meet the symmetry

$$\begin{aligned} & R: (x_2, x_4, x_5, x_6, \sin\theta, \sin 2(\phi-\gamma)) \to (x_2, -x_4, x_5, x_6, \sin\theta, -\sin 2(\phi-\gamma)), \\ & \quad t \to -t \quad (h \to -h). \end{aligned} \tag{31}$$

Considering the homoclinic boundary conditions, make the values of K_1 and K_3 into

$$K_1 = m^2, K_3 = 1. \tag{32}$$

And K_2 is a free parameter which is used to adjust the energy H of energy balance oscillator. We also have

$$\tilde{h} = \frac{m^2 x_4}{\tilde{r}}(\tilde{r}x_5\sin\theta + \tilde{r}x_6\cos\theta - 3\sin\theta\cos\theta), \tag{33}$$

and $\tilde{f}(\theta)$,

$$\begin{aligned}\tilde{f}(\theta)=\frac{1}{\tilde{r}^3}[&(5\tilde{r}\sin\theta-15\tilde{r}\sin\theta\cos^2\theta)K_1-(6m^2\tilde{r}^2-12m^2\tilde{r}^2\cos^2\theta)K_2\\&-(\tilde{r}^3\sin\theta+10m^2\tilde{r}\sin\theta\cos\theta-20m^2\tilde{r}\sin\theta\cos^3\theta)K_3\\&+(4m^2\tilde{r}^2+3m^2\tilde{r}^2\nu-8m^2\tilde{r}^2\cos^2\theta-6m^2\tilde{r}^2\nu\cos^2\theta)K_3^2\\&+\tilde{r}^2\cos\theta K_1K_3-2m^2+9\tilde{r}^2\cos\theta+16m^2\cos^2\theta\\&-15\tilde{r}^2\cos^3\theta-26m^2\cos^4\theta+12m^2\cos^6\theta.\end{aligned} \tag{34}$$

Equation (27) contains rich physical phenomena. Consider the initial conditions of $\theta(0)=0,\ \dot{\theta}(0)=0$, through numerical analysis, we can see that equation has two critical points respectively, which will produce the phenomenon of heteroclinic orbits, when $0\le\tilde{r}\le0.9648$ and $1.9093\le\tilde{r}\le2$. Taking $\tilde{r}=0.8$ for example, the system (27) has two critical load $m_{c1}=1.1177$ and $m_{c1}=1.9499$. The second case is analyzed in this paper and its potential energy curves and phase diagram are shown in Figure 3(a). Most of the existing literature only simulated one homoclinic orbit of system (27) using numerical method and do not analyze the phenomenon of heteroclinic orbits in detail. In the next section, we will apply the analytical method that calculated analytical heteroclinic orbits in two typical critical stats. Heteroclinic solutions and its corresponding 3D configuration and internal force diagrams are obtained respectively.

Let

$$p=\cos\theta. \tag{35}$$

When $0<\theta<\pi$, the original equation (27) can be simplified as follows,

$$\begin{aligned}&\frac{1}{2}\dot{p}^2+\frac{p}{m^2}+(\frac{3}{2\tilde{r}^2}+K_2-\frac{1}{2}K_3^2(1+\nu))p^2-\frac{1}{m^2}p^3\\&-\frac{3}{2\tilde{r}^2}p^4+\frac{1}{2\tilde{r}^2}p^6-(K_2-\frac{1}{2}K_3^2(1+\nu)+\frac{1}{2\tilde{r}^2})\\&+(\frac{K_1}{\tilde{r}m^2}-\frac{K_3}{\tilde{r}}p-\frac{K_1}{\tilde{r}m^2}p^2+\frac{K_3}{\tilde{r}}p^3)\sqrt{1-p^2}=0.\end{aligned} \tag{36}$$

Differentiating both ends of the equation, we can get a second-order differential equation

$$\begin{aligned}&\ddot{p}+\frac{1}{m^2}+(\frac{2}{m^2}+\frac{3}{\tilde{r}^2})p-\frac{3}{m^2}p^2-\frac{6}{\tilde{r}^2}p^3+\frac{3}{\tilde{r}^2}p^5\\&-(\frac{1}{\tilde{r}}+\frac{3}{\tilde{r}}p-\frac{5}{\tilde{r}}p^2-\frac{3}{\tilde{r}}p^3+\frac{4}{\tilde{r}}p^4)\frac{1}{\sqrt{1-p^2}}=0.\end{aligned} \tag{37}$$

When $-\pi<\theta<0$, $\sin\theta=-\sqrt{1-p}$. Simplified equation also can be obtained by using similar solution method, so the detailed solving procedure is not explained again.

4. Padé approximation

Extended Padé approximation method has been successfully used to solve the heteroclinic orbits of asymmetric system. The extended Padé approximation is implemented here. Set the series solution of equation (37) to

$$x(t)=a_0+a_1s+\cdots=\sum_{n=0}^{\infty}a_ns^n\ . \tag{38}$$

Initial point values of the track are represented as (a_0,a_1), and a_0,a_1 are not zero at the same time,

$$x(0)=a_0,\qquad \dot{x}(0)=a_1. \tag{39}$$

Other parameters can be expressed as a function of a_0,a_1,r,m:

$$
\begin{aligned}
a_2 &= \frac{1}{2m^4r^4}(-m^2r^4 - 3m^4r^2a_0 - 2m^2r^4a_0 + 3m^2r^4a_0^2 + 6m^4r^2a_0^3 \\
&\quad + \sqrt{(m^8r^6 + 6m^8r^6a_0 - 30m^8r^6a_0^3 + 15m^8r^6a_0^4 + 24m^8r^6a_0^5 - 16m^8r^6a_0^6)}) \\
&\quad - 3m^4r^2a_0^5, \\
a_3 &= (-3m^2r^2a_1 + 3m^4r^2a_1 - 9m^4a_0a_1 - 12m^2r^2a_0a_1 + 45m^2r^2a_0^2a_1 \\
&\quad - 45m^4r^2a_0^2a_1 + 18r^4a_0^2a_1 + 72m^4a_0^3a_1 + 48m^2r^2a_0^3a_1 + 30m^4r^2a_0^3a_1 \\
&\quad - 18r^4a_0^3a_1 - 105m^2r^2a_0^4a_1 + 60m^4r^2a_0^4a_1 - 162m^4a_0^5a_1 - 36m^2r^2a_0^5a_1 \\
&\quad - 48m^4r^2a_0^5a_1 + 63m^2r^2a_0^6a_1 + 144m^4a_0^7a_1 - 45m^4a_0^9a_1 - 6m^4r^2a_1a_2 \\
&\quad - 4m^2r^4a_1a_2 + 12m^2r^4a_0a_1a_2 + 36m^4r^2a_0^2a_1a_2 - 30m^4r^2a_0^4a_1a_2) \\
&\quad - 2r^4a_1 + 2r^4a_0a_1/(6m^2r^2(r^2 + 3m^2a_0 + 2r^2a_0 - 3r^2a_0^2 - 6m^2a_0^3 \\
&\quad + 3m^2a_0^5 + 2m^2r^2a_2), \\
&\cdots
\end{aligned}
\tag{40}
$$

4.1. Homoclinic and heteroclinic orbits

Transformed system (37) has homoclinic and heteroclinic orbits at same time, when $r = 0.8, m_{c1} = 1.94988$. Potential energy curve and phase diagram are shown in Figure 3(b), wherein solid lines indicate the graphics of system (37) at $0 < \theta < \pi$ and dashed lines at $-\pi < \theta < 0$. The results at $0 < \theta < \pi$ are analyzed here. Phase diagram has one homoclinic orbit and two heteroclinic orbits which are symmetric about the p-axis but not symmetric about the $\dot{p}$-axis. As shown that H_1 and H_2 are two saddle points, and O is center. When $s \to +\infty$, point on homoclinic orbits move along H_1AH_2 and finally tend to reach saddle point H_1, and point on heteroclinic orbits movement along $H_1B_1H_2$ and $H_2B_2H_1$ respectively and finally tend to reach the corresponding saddle point H_1 and H_2; when $s \to -\infty$, along the opposite direction to the other saddle point.

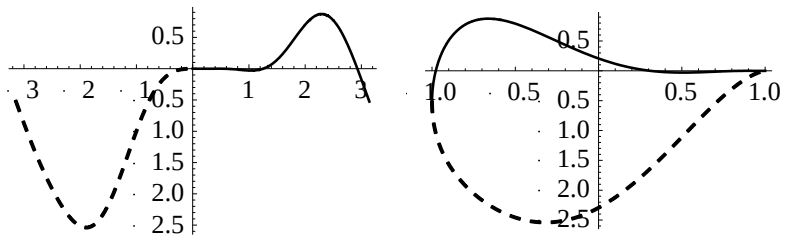

(a) system (27)

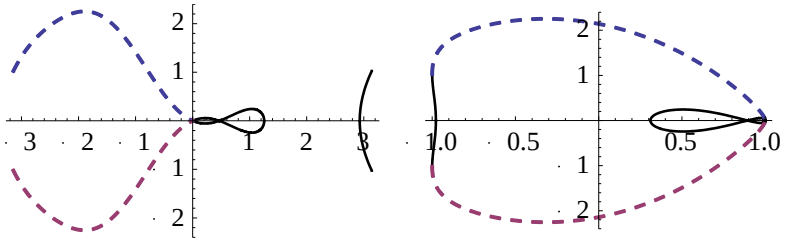

(b) system (37)

Figure 3 Potential energy curve and phase diagram

Take an initial vales are maximum point at p-axis, which meet its tangent perpendicular to the p-axis, namely

$$a_2 = 0. \tag{41}$$

Form of homoclinic solution is

$$PA = \frac{(\alpha_0 + \alpha_1 t + \alpha_2 t^2 + \alpha_3 t^3 + \alpha_4 t^4)}{(1 + \beta_1 t + \beta_2 t^2 + \beta_3 t^3 + \beta_4 t^4)}. \tag{42}$$

All the coefficients of PA_n are obtained by comparing the PA_n and Taylor expansion solution, namely

$$\sum_{n=0}^{\infty} a_n t^n \cong PA_n. \tag{43}$$

Then consider the convergence condition:

$$\lim_{x\to\infty} PA \to H. \tag{44}$$

The other parameters can be expressed by the algebraic polynomial as a_0, a_1 either. And used the convergence condition, the initial value can be obtained respectively. We obtain the initial values $a_0 = 0.310214$, and fourth-order approximation homoclinic solution,

$$p = \frac{0.310214 + 0.257087 s^2 + 0.0365497 s^4}{1 + 0.347095 s^2 + 0.0409154 s^4}. \tag{45}$$

Take initial vales at the maximum point of $\dot{p}$-axis, which also meet its tangent perpendicular to the $\dot{p}$-axis, namely

$$a_3 = 0. \tag{46}$$

Form of heteroclinic solution is

$$QPA = \frac{(\alpha_0 + \alpha_1 \mathrm{e}^{\sqrt{\omega}t} + \alpha_2 \mathrm{e}^{2\sqrt{\omega}t} + \alpha_3 \mathrm{e}^{3\sqrt{\omega}t} + \alpha_4 \mathrm{e}^{4\sqrt{\omega}t})}{(1 + \mathrm{e}^{\sqrt{\omega}t}\beta_1 + \mathrm{e}^{2\sqrt{\omega}t}\beta_2 + \mathrm{e}^{3\sqrt{\omega}t}\beta_3 + \mathrm{e}^{4\sqrt{\omega}t}\beta_4)}, \tag{47}$$

where ω is etermined as the coefficient to be solved. Calculation process is resembled to precious solution. Convergence condition (44) is considered, and then initial value $a_1 = \pm 0.0145213, \omega = 0.170252$ and heteroclinic solution can be obtained

$$\begin{aligned} p^{+} &= \frac{0.8933 + 4.06384 e^{0.412616 s} + 3.89703 e^{0.825232 s} + 1.61965 e^{1.23785 s} + 0.268084 e^{1.65046 s}}{1 + 4.06384 e^{0.412616 s} + 3.89703 e^{0.825232 s} + 1.61965 e^{1.23785 s} + 0.268084 e^{1.65046 s}}, \\ p^{-} &= \frac{1 + 6.04159 e^{0.412616 s} + 14.5366 e^{0.825232 s} + 15.1588 e^{1.23785 s} + 3.33217 e^{1.65046 s}}{1 + 6.04002 e^{0.412616 s} + 14.6258 e^{0.825232 s} + 16.5536 e^{1.23785 s} + 3.73018 e^{1.65046 s}}. \end{aligned} \tag{48}$$

The calculated position of the saddle point is 0.8933 and 1 which are identical with exact values. Compare present solution of homoclinic and heteroclinic solutions about arc length s and homoclinic and heteroclinic orbits with numerical solution as shown in Figure 4 - 6.

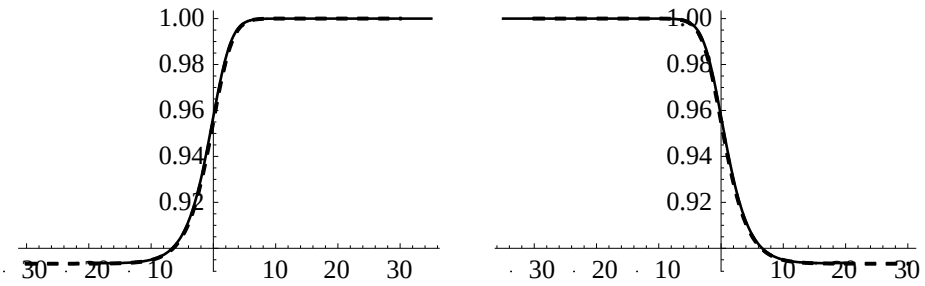

(a) $a_1 > 0$ (b) $a_1 < 0$

Figure 4 heteroclinic solution

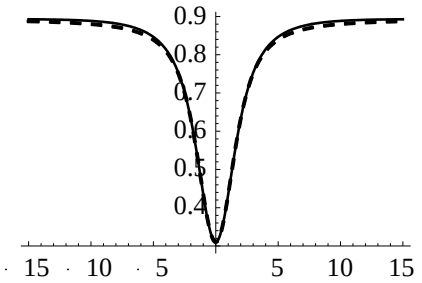

Figure 5 homoclinic solution

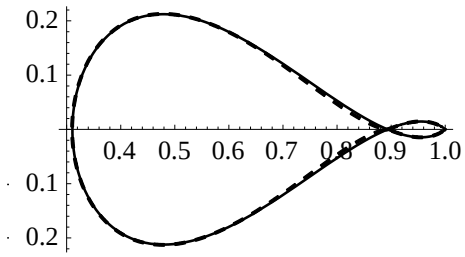

Figure 6 homoclinic and heteroclinic orbits

The rod of internal force and 3D configuration can be obtained respectively. When $s \to \infty$, homoclinic orbit appears, θ is gradually decreased from 1.25538 to 0.466162 and then remains constant. In the corresponding 3D configuration, rotation angle, beginning with the location of the initial point 0.315416, gradually increases to 1.10463, then spiral extends to the right endsand hang with this angle, while the state of rod remain stretching. The axial force of rod has maximum value located at initial point and point to outer cylinder. As $s \to \infty$, axial force gradually decreases to zero. As shown in Figure 7, rotational angle of the rod increases to the ends and spiral extending with constant angle. When heteroclinic orbits appear, taking $a_1 > 0$ for example. When $s \to +\infty$, θ is gradually changed from 0.300549 to 0.466162 and then remains constant; when $s \to -\infty$, θ is gradually changed from 0.300549 to 0 and also remains constant. In the corresponding 3D configuration, rotation angle, beginning with the location of the initial point 1.27025, gradually decreases to 1.10463, while state remains stretching. Rotation angle gradually increase to $\pi/2$, namely changed to horizontally extending. The axial force of rod has maximum value in the location of initial point and point to inner cylinder. As $s \to -\infty$, axial force of rod change to point to outer cylinder, and then decreases to zero; as $s \to +\infty$, axial force also has a related change and finally reach to 0.0181901. As shown in Figure 8, at one end rotational angle of the rod increases and spiral extending with constant angle, at other end it extends horizontally. When $a_1 < 0$, the process is similar to the above.

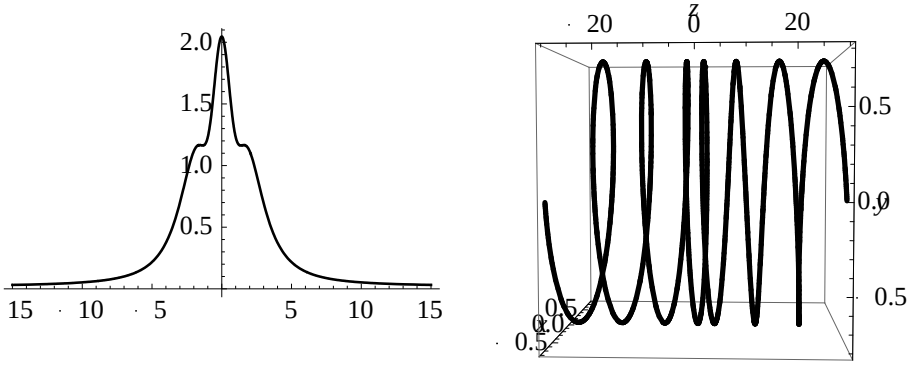

Figure 7 internal force and 3D configuration (homoclinic solution)

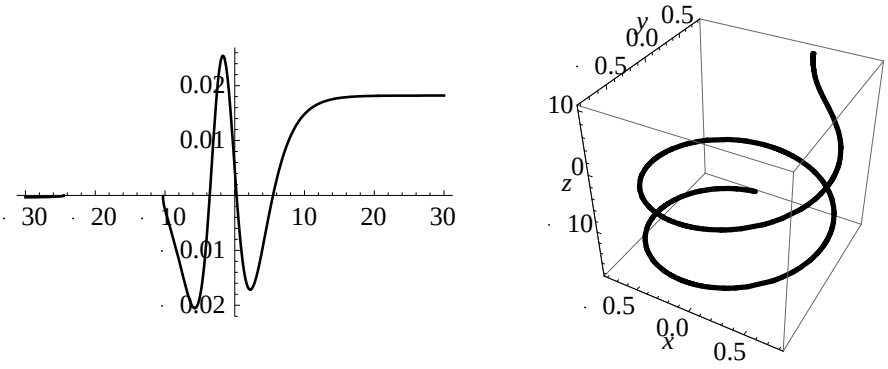

Figure 8 internal force and 3D configuration (heteroclinic solution $a_1 > 0$)

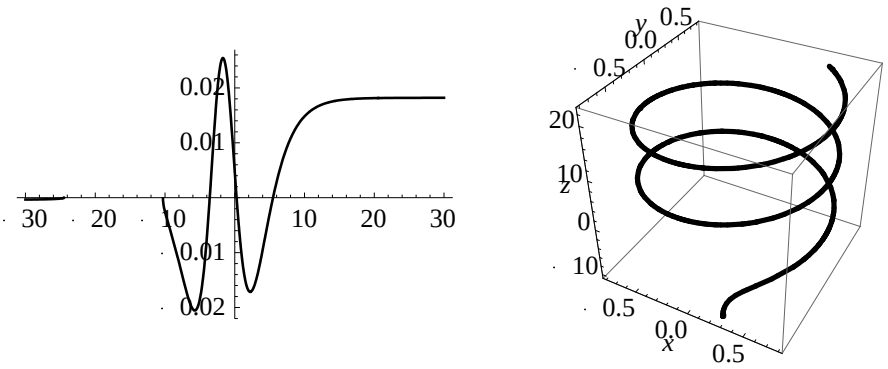

Figure 9 internal force and 3D configuration (heteroclinic solution $a_1 < 0$)

5. Conclusions

This paper presents the general formulation of a twisted rod constrained to lie on an elliptic cylinder. On the statics of twisted rods, much headway has been made by dynamical systems analogy, and homoclinic and heteroclinic orbits are analyzed to describe localized buckling modes of long rods. The strategy presented in this work is generally applied and accepted, so it would be possible to apply the present method to simulate heterogeneity of the protein molecules with more complicated nonlinearity which will be the topic for further research.

By developing the Padé approximation method, the homoclinic and heteroclinic orbits of nonlinear irrational equations can be constructed, which would expand the ranges of the applicable systems, and also can be applied to improve the accuracy of the result. It is feasible to apply this method on the other complex systems; furthermore, by using the combination of high order Melnikov method and improved Padé approximation method, the accuracy of calculation can be improved even further.

Conclusions

Project supported by National Natural Science Foundation of China (Grant No. 11072168, 11102127), Specialized Research Fund for the Doctoral Program of Higher Education of China (Grant No. 20100032120006) and Tianjin Research Program of Application Foundation and Advanced Technology (12JCYBJC12500, 12JCZDJC28000).

References

[1] Bedrossian A N, Abbassian F, Dunayevsky V A and Hope S A. *Analysis of post-buckling behaviour of drillstrings*. in *8th U.K. ABAQUS User Group Conference*. 1993.
[2] Paslay P R and Bogy D B 1964 The stability of a circular rod laterally constrained to be in contact with an inclined circular cylinder *Joural of applied mechanics-transactions of the ASME* **31** 605-10
[3] Heijden G H M, Champneys A R and Thompson J M T 1998 The spatial complexity of localized buckling in rods with noncircular crosssection *SIAM J. Appl. Math.* **59** 198-221
[4] Van Der Heijden G H M and Thompson J M T 1998 Lock-on to tape-like behaviour in the torsional buckling of anisotropic rods *Physica D* **112** 201-24
[5] Van Der Heijden G H M 2001 The static deformation of a twisted elastic rod constrained to lie on a cylinder *Proceedings of the Royal Society A: Mathematical, Physical and Engineering Sciences* **457** 695-715
[6] Van Der Heijden G H M, Champneys A R and Thompson J M T 2002 Spatially complex localisation in twisted elastic rods constrained to a cylinder *Int. J. Solids Struct.* **39** 1863-83
[7] Van Der Heijden G H M, Champneys A R and Thompson J M T 1999 Spatially complex localisation in twisted elastic rods constrained to lie in the plane *Jouranl of the mechanics and physics of solids* **47** 59-79
[8] Emaci E, Vakakis A F, Andrianov I V and Mikhlin Y 1997 Study of two-dimensional axisymmetric breathers using Pade approximants *Nonlinear Dyn.* **13** 327-38
[9] Mikhlin Y V 2000 Analytical Construction of Homoclinic Orbits of Two- and Three-Dimensional Dynamical Systems *J. Sound Vib.* **230** 971-83
[10] Manucharyan G V and Mikhlin Y V 2005 The construction of homo- and heteroclinic orbits in non-linear systems *J. Appl. Math. Mech.* **69** 39-48
[11] Feng J J, Zhang Q C and Wang W 2011 The construction of homoclinic and heteroclinic orbitals in asymmetric strongly nonlinear systems based on the Pade approximant *Chin. Phys. B* **20** 090202
[12] Feng J J, Zhang Q C and Wang W 2012 Chaos of several typical asymmetric systems *Chaos, Solitons Fractals* **45** 950-58
[13] Zhang Q C, Feng J J and Wang W 2011 The construction of homoclinic and heteroclinic orbit in two-dimentsional nonlinear systems based on the quasi-Pade approximation *Chinese Journal of Theoretical and Applied Mechani* **43** 914-21
[14] Antman S S 1995 *Nonlinear problems of elasticity* Springer